Research Article Vol. 5, No. 7 / July 2018 / Optica 774

# Ultrafast rogue wave patterns in fiber lasers

Avi Klein,[1,†] Gilad Masri,[1,†] Hamootal Duadi,[1] Kfir Sulimany,[2] Ohad Lib,[2] Hadar Steinberg,[2] Stanislav A. Kolpakov,[3] and Moti Fridman[1,*]

[1]Faculty of Engineering and the Institute of Nanotechnology and Advanced Materials, Bar-Ilan University, Ramat Gan 5290002, Israel
[2]The Racah Institute of Physics, The Hebrew University of Jerusalem, Jerusalem, Israel
[3]School of Engineering and Applied Science, Aston University, Aston Triangle, Birmingham B4 7ET, UK
*Corresponding author: mordechai.fridman@biu.ac.il

Received 18 January 2018; revised 18 March 2018; accepted 3 April 2018 (Doc. ID 320155); published 26 June 2018

**Fiber lasers are convenient for studying extreme and rare events, such as rogue waves, thanks to the lasers' fast dynamics. Indeed, several types of rogue wave patterns were observed in fiber lasers at different time-scales: single peak, twin peak, and triple peak. We measured the statistics of these ultrafast rogue wave patterns with a time lens and developed a numerical model proving that the patterns of the ultrafast rogue waves were generated by the non-instantaneous relaxation of the saturable absorber together with the polarization mode dispersion of the cavity. Our results indicate that the dynamics of the saturable absorber is directly related to the dynamics of ultrafast extreme events in lasers.** 

***OCIS codes:*** (060.7140) Ultrafast processes in fibers; (060.5530) Pulse propagation and temporal solitons; (060.4370) Nonlinear optics, fibers; (060.3510) Lasers, fiber.

https://doi.org/10.1364/OPTICA.5.000774

## 1. INTRODUCTION

Extreme events, and in particular rogue waves, play an important role in the dynamics of numerous physical systems, e.g., oceanography, where rogue waves endanger life and cargo [1]; atmospheric science [2]; Bose–Einstein condensation [3]; and optical rogue waves in nonlinear media [4]. Optical rogue waves serve as a useful test bench, thanks to their fast dynamics, which makes it possible to measure extreme events in a short time and under a controlled environment [4–7]. These waves result from the fiber nonlinearity, which is governed by the nonlinear Schrödinger equation (NLSE), and exhibit a vast variety of patterns [8–21]. Fiber lasers are far richer systems than nonlinear fibers, because the gain competition and saturable absorber give rise to unique rogue waves. In addition, the rogue waves in fiber lasers can be measured after each round trip to reveal their dynamics [4,7].

Three types of rogue waves appear in fiber lasers at different time scales: slow rogue waves at seconds to microseconds, fast rogue waves at hundreds of nanoseconds to tens of picoseconds, and ultrafast rogue waves at picoseconds and faster. Slow rogue waves are generated from the gain nonlinearity under pump modulation, which leads to hopping between two attractors according to the laser rate equations [22–26]. Fast rogue waves are generated from polarization instabilities and are usually attributed to soliton–soliton interactions governed by the NLSE [27–29]. Both slow and fast rogue waves have been thoroughly investigated in recent years and have shown a variety of patterns that agree with numerical models. However, although it is relatively easy to measure slow and fast rogue waves, it is challenging to measure ultrafast rogue waves, because electronic detectors have limited time resolution [30–33].

Two methods for measuring ultrafast rogue waves were developed: time stretching and time lensing. In time stretching, the Fourier transform of the signal is measured in real time, but the phase must be guessed to restore the signal [34–41]. In time lensing, the signal is imaged but must be synchronized for a specific timing [42–48]. Combination of these two methods enabled real-time measurement of both the intensity and phase of rogue waves and revealed different temporal patterns [49–52]. However, the statistics of the patterns are still unknown, and numerical simulations to date have failed to reproduce these temporal structures [26,53–56]. Both the statistics and numerical simulations are essential for bridging the experimental results and the analytical solutions.

In this work, we investigated the temporal structure of a large number of ultrafast rogue waves and obtained statistics for single-peak, twin-peak, and triple-peak patterns. In addition, we developed a numerical model simulating these patterns. Our results establish that one of the sources of ultrafast rogue wave patterns is the non-instantaneous nature of the saturable absorber together with the polarization mode dispersion (PMD) of the fiber, indicating that the mechanism generating ultrafast rogue waves differs from that generating slow or fast rogue waves. This mechanism suggests the possibility of realizing unique analytic solutions of rogue waves, such as triangular rogue waves or triplet rogue waves [10,12].

## 2. METHODS AND MEASUREMENTS

A schematic of the experiment is shown in Fig. 1. An erbium-doped pulsed fiber laser with a graphene sheet as a saturable absorber is used. When operating under stable conditions, it emits a train of pulses separated by 80 ns with a 3 nm bandwidth and 1 ps pulse width, as shown in insets (a) and (b). When the laser is set to unstable conditions, at specific states of polarization and at power levels that are three times the threshold, the field fluctuates. The fluctuation along with the intrinsic nonlinearity and the dispersion of the cavity lead to rare events with intensities much higher than the average, which were identified as rogue waves [57].

First, we measured the intensity distribution of 50,000 pulses, as shown in Fig. 2 on a log scale. The distribution has an L shape, indicating that extreme events are more frequent than expected for a normal distribution, which is shown by the red dashed curve [4]. The rogue wave threshold was defined as twice the significant wave height, which is calculated as the mean amplitude of the highest third of the waves and shown as a yellow dashed line [26,58]. The inset of Fig. 2 shows a typical measurement of the laser output noise for 50 different round trips, where three rogue waves are observed.

We measured the rogue waves using a temporal magnification scheme with a 400 fs resolution [43,44,59] and analyzed the pattern of each rogue wave. We found three types of rogue wave patterns: single-peak, twin-peak, and triple-peak patterns, as illustrated in the upper insets of Fig. 3. The probability of each pattern, shown in Fig. 3, increased with the pump power until a maximum was reached at 360 mW, after which it decreased; this is similar to the number of slow rogue waves in random lasers [60]. The single-peak patterns were found to be most frequent, but the twin-peak and triple-peak patterns also accounted for a significant portion of all the rogue waves.

The temporal magnification scheme was synchronized to the laser repetition rate, so the same pattern could be measured after each round trip. This makes it possible to distinguish between multipeak and single-peak patterns. The peak separation in the twin-peak and triple-peak rogue waves was stable as the rogue waves propagated in the cavity, whereas the separation between single-peak rogue waves changed after each round trip owing to the PMD. Typical measured results for the separation between two peaks are presented in Fig. 4. The red circles show a stable

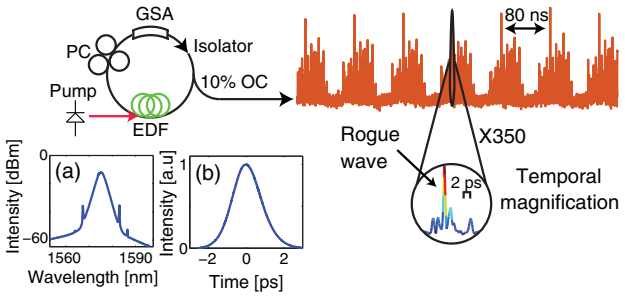


**Fig. 1.** Rogue wave measurement scheme with 350× temporal magnification. Insets (a) and (b) show the laser spectrum and measured pulse width of 1 ps during operation under stable conditions, respectively. The red curve shows the measured low-resolution output under unstable conditions, which reveals the generation of a rogue wave from the intensity noise. GSA, graphene saturable absorber; OC, output coupler; EDF, erbium-doped fiber; PC, polarization controller.

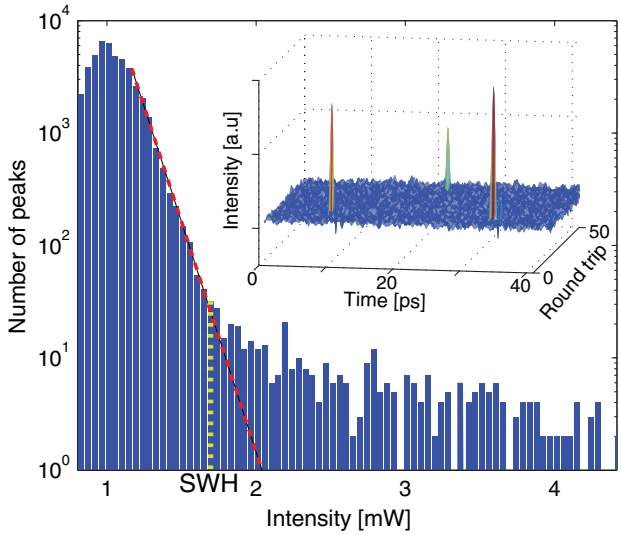


**Fig. 2.** Histogram of the peak intensities; the large tail deviates from the exponential distribution predicted by stochastic models (red dashed curve). SWH: significant wave height. Inset: high-resolution measurement of the laser output noise showing three rogue waves.

10 ps separation between the peaks over eight round trips, indicating a twin-peak pattern, as shown in the inset. The blue squares show an increasing separation between peaks, indicating two separate single-peak rogue waves that happened to be close to each other. It is possible to measure the dynamics of the rogue waves over a large number of round trips with lower temporal resolution or over a small number of round trips with higher resolution.

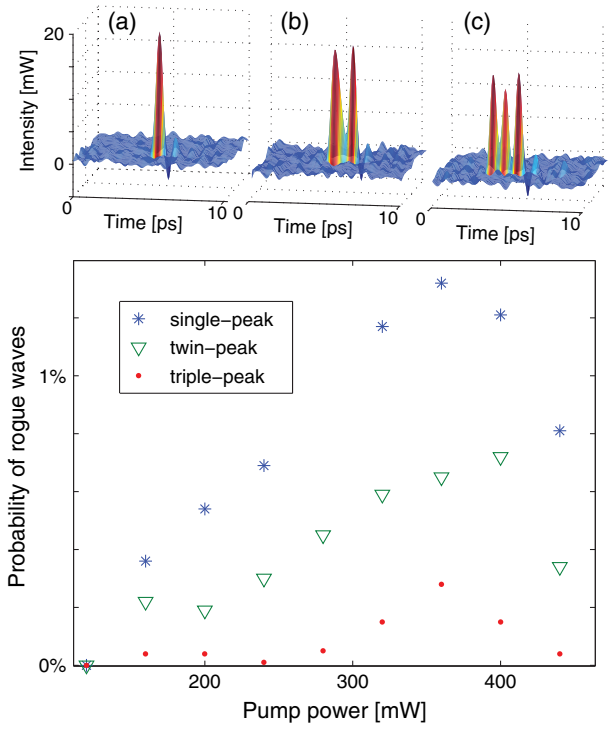


**Fig. 3.** Probability of rogue waves as a function of the laser pump power for single-peak, twin-peak, and triple-peak patterns. Insets show typical measured results of each rogue wave pattern.

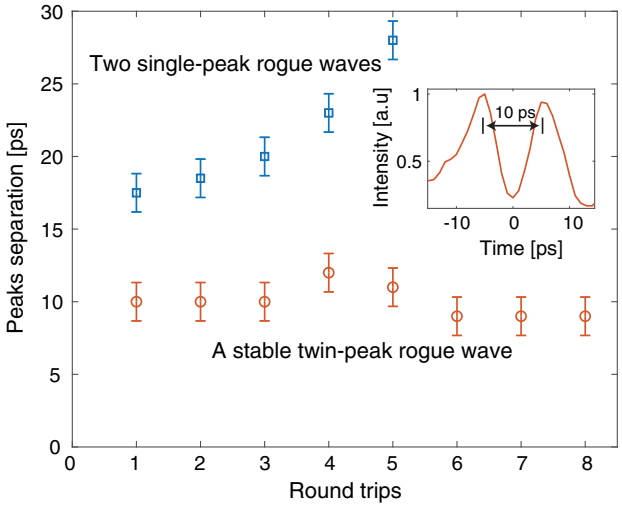


**Fig. 4.** Measured separation between peaks as a function of the number of round trips in the cavity for two cases: stable separation, indicating a twin-peak pattern (circles), and increasing separation, indicating two separate single-peak rogue waves. Inset illustrates the stable twin-peak rogue wave.

A comparison of our results to those for slow and fast rogue waves revealed that the rogue waves we observed were the result of a different underlying mechanism. Slow rogue waves emerge because of the gain nonlinearities and are observed at time scales from seconds to milliseconds [22–26], whereas our rogue waves were shorter by at least 9 orders of magnitude. Fast rogue waves emerge because of soliton–soliton interaction and are observed close to the laser threshold [24,27–29], whereas the maximum number of rogue waves in our study was measured at a pump power that was three times the lasing threshold. Therefore, we attribute our rogue waves to the non-instantaneous response of the saturable absorber. To establish this hypothesis, we developed a numerical model of the laser cavity and compared the calculated results with the experimental measurements.

## 3. NUMERICAL SIMULATIONS

To simulate the laser, we extended the numerical model presented in [31] to include PMD, vector field propagation, and a non-instantaneous saturable absorber. The propagation of the vector field envelope was simulated in each element of the fiber laser and repeated over a large number of round trips. The field envelope $\vec{\psi} = \{\psi_x, \psi_y\}$ traveling in a dispersive nonlinear fiber was governed by the NLSE:

$$i\vec{\psi}_z + \frac{D}{2}\vec{\psi}_{tt} + |\vec{\psi}|^2\vec{\psi} = 0, \tag{1}$$

where $D$ represents the dispersion tensor of the fiber with different values for each component of the field owing to PMD, $z$ is the propagation distance, and $t$ is the time in a moving frame of reference with the group velocity.

The erbium-doped fiber (EDF) was simulated by

$$i\vec{\psi}_z + \frac{D_2}{2}\vec{\psi}_{tt} + \Gamma_2|\vec{\psi}|^2\vec{\psi} = \frac{ig_0}{1 + Q/Q_{\text{sat}}}(\vec{\psi} + \beta_2\vec{\psi}_{tt}), \tag{2}$$

where $Q_{\text{sat}}$ represents the saturation energy, $g_0$ is the small-signal gain, $\beta_2$ is the spectral width of the gain, $\Gamma_2$ is the nonlinear coefficient, and the total energy $Q$ is

$$Q = \int_{-\infty}^{\infty} |\vec{\psi}|^2 \mathrm{d}t. \tag{3}$$

The instantaneous saturable absorber was modeled by

$$T(t) = T_0 + \Delta T \frac{I(t)}{I_{\text{sat}} + I(t)}, \tag{4}$$

where $I(t) = |\vec{\psi}|^2$, $T_0$ is the transmission for a low-intensity optical field, and $I_{\text{sat}}$ is the saturation intensity. To include the response time of the saturable absorber, we imposed a low-pass filter with a cutoff frequency of 1 THz on $T(t)$ [61,62].

The propagation in the fiber laser follows the principal states of polarization (PSP) in the cavity, and the polarization controller couples the two PSPs according to

$$\vec{\psi}_{\text{out}} = \begin{bmatrix} (1-\kappa)e^{i\varphi_1} & \kappa e^{i\varphi_2} \\ \kappa e^{-i\varphi_2} & (1-\kappa)e^{-i\varphi_1} \end{bmatrix} \vec{\psi}_{\text{in}}, \tag{5}$$

where $\kappa$ is the coupling strength, $\varphi_1$ is the relative phase between the two states of polarization, and $\varphi_2$ is the cross phase.

Using these numerical tools, we first simulated the propagation of the vector field envelope in the fiber laser as a function of the PMD value without the low-pass filter. At low values of the PMD, the field envelope in the fiber laser was chaotic, as shown in Fig. 5(a); this is similar to the results of scalar calculations [31]. When the PMD in the fiber was increased, the chaotic pulsation evolved into high peaks that appeared once every few hundred round trips, as shown in Figs. 5(b) and 5(c). These results indicated that including the PMD leads to the generation of rogue waves in ring fiber cavities.

Next, we included the non-instantaneous relaxation of the saturable absorber by introducing a low-pass filter on $T(t)$ in Eq. (4). This leads to twin-peak and triple-peak patterns, as shown in Figs. 6(b) and 6(c), where multiple peaks were observed with stable separation between them as a function of the number of round trips. We counted the number of multipeak patterns as a function of the low-pass filter cutoff frequency and evaluated their

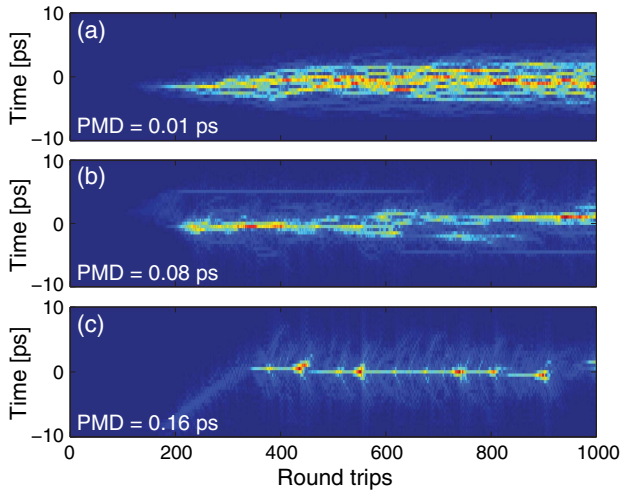


**Fig. 5.** Calculated vector field envelope as a function of the number of round trips in the fiber laser for different PMD values. (a) Low PMD, showing the same chaotic behavior as a scalar model. (b) Increased PMD, showing fewer pulses. (c) Realistic value of PMD, showing rogue waves every few hundred round trips. $L_{\text{smf}} = 10$, $L_{\text{edf}} = 0.22$, $D_2 = -0.735$, $\Gamma_2 = 3$, $g_0 = 4$, $\beta_2 = 0.008$, $Q_{\text{sat}} = 8$, $T_r = 0.7$, $T_0 = 0.9$, $\Delta T = 0.1$, $I_{\text{sat}} = 0.6$, $\kappa = 0.2$, $\varphi_1 = 0$, and $\varphi_2 = 0.1$.

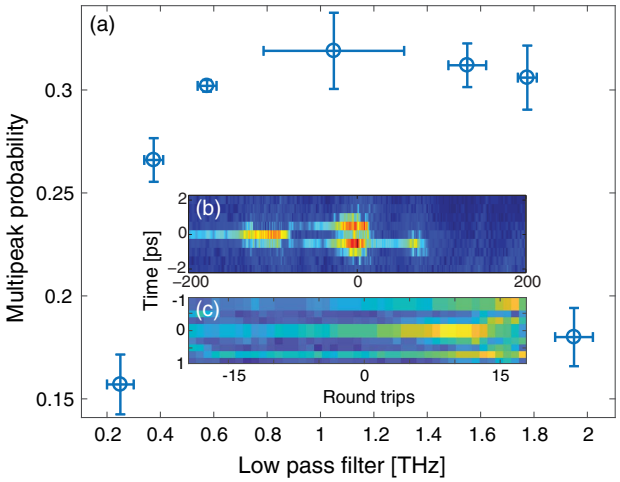


**Fig. 6.** (a) Probability of multipeak rogue waves as a function of the cutoff frequency of the low-pass filter. (b) and (c) Typical calculated twin-peak and triple-peak rogue waves, respectively.

probability by comparing it to that of single-peak rogue waves, as shown in Fig. 6(a). The results indicate that the maximum number of multipeak rogue waves was obtained at a 1 THz cutoff frequency, which is on the order of the response time of our graphene saturable absorber [61,62].

We evaluated the likelihood of single-peak, twin-peak, and triple-peak patterns as a function of $Q_{sat}$, as shown in Fig. 7(e). When $Q_{sat} = 3$, which is close to the laser threshold, no rogue waves appeared, as shown in Fig. 7(a). When $Q_{sat}$ was increased, high peaks appeared [Fig. 7(b)], and their amplitude distribution deviated from an exponential distribution [Fig. 7(c)], indicating that they were rogue waves. When $Q_{sat}$ was further increased, more peaks appeared, but their distribution followed an exponential distribution [Fig. 7(d)], indicating that the peaks were not rogue waves. The ratio between the single-peak, twin-peak, and triple-peak patterns was consistent with the measured results of Fig. 3 and with previously published results [60]. These calculated results establish that the underlying mechanism of our rogue waves is the non-instantaneous response of the saturable absorber together with the PMD of the cavity. The bars illustrate the standard deviations calculated from 20 independent simulations for each point.

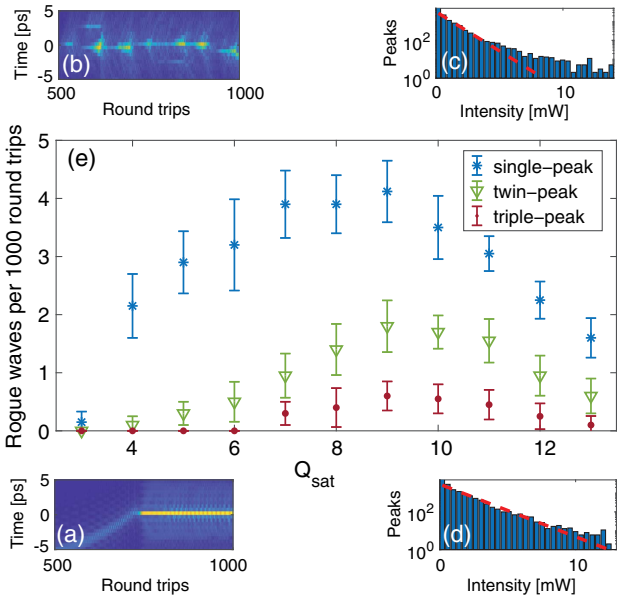


**Fig. 7.** (e) Calculated likelihood of rogue waves in the simulation as a function of $Q_{sat}$. (a) Typical output as a function of time for $Q_{sat} = 3$, (b) typical output as a function of time for $Q_{sat} = 8$, (c) peak height histogram for $Q_{sat} = 8$, which deviates from an exponential distribution (dashed line), and (d) peak height histogram for $Q_{sat} = 13$, which shows an exponential distribution (dashed line).

## 4. CONCLUSIONS

To conclude, we acquired the statistics of the temporal structure of ultrafast rogue waves and developed a numerical model that agrees with the measured results. We showed that rogue waves appeared only when we considered both the PMD of the cavity and the non-instantaneous relaxation of the saturable absorber. These results indicate that the mechanism governing the ultrafast rogue wave dynamics in pulsed fiber lasers is neither attractor hopping nor soliton–soliton interaction but arises from the temporal behavior of the saturable absorber together with the PMD of the cavity.

**Funding.** Leverhulme Trust (RPG-2014-304); ERASME (745556 PANDA); Israel Science Foundation (ISF) (1363/15).

**Acknowledgment.** S. A. K. is grateful for a Leverhulme Trust Grant and an ERASME grant. H. S. acknowledges support from the Israeli Science Foundation.

†These authors contributed equally to this work.

## REFERENCES

1. K. Dysthe, H. E. Krogstad, and P. Müller, "Oceanic rogue waves," Annu. Rev. Fluid Mech. **40**, 287–310 (2008).
2. S. El-Labany, W. Moslem, N. El-Bedwehy, R. Sabry, and H. A. El-Razek, "Rogue wave in Titan's atmosphere," Astrophys. Space Sci. **338**, 3–8 (2012).
3. Y. V. Bludov, V. V. Konotop, and N. Akhmediev, "Matter rogue waves," Phys. Rev. A **80**, 033610 (2009).
4. N. Akhmediev, B. Kibler, F. Baronio, M. Belić, W.-P. Zhong, Y. Zhang, W. Chang, J. M. Soto-Crespo, P. Vouzas, P. Grelu, C. Lecaplain, K. Hammani, S. Rica, A. Picoxxi, M. Tlidi, K. Panajotov, A. Mussor, A. Bendahmane, P. Szriftgiser, G. Genty, J. Dudley, A. Kudlinski, A. Demircan, U. Morgner, S. Amiraranashvili, C. Bree, G. Steinmeyer, C. Masoller, N. G. R. Broderick, A. F. J. Runge, M. Erkintalo, S. Residori, U. Bortolozzo, F. T. Arecchi, S. Wabnitz, C. G. Tiofack, S. Coulibaly, and M. Taki, "Roadmap on optical rogue waves and extreme events," J. Opt. **18**, 063001 (2016).
5. D. Solli, C. Ropers, P. Koonath, and B. Jalali, "Optical rogue waves," Nature **450**, 1054–1057 (2007).
6. D.-I. Yeom and B. J. Eggleton, "Photonics: rogue waves surface in light," Nature **450**, 953–954 (2007).
7. J. M. Dudley, F. Dias, M. Erkintalo, and G. Genty, "Instabilities, breathers and rogue waves in optics," Nat. Photonics **8**, 755–764 (2014).
8. A. Armaroli, C. Conti, and F. Biancalana, "Rogue solitons in optical fibers: a dynamical process in a complex energy landscape?" Optica **2**, 497–504 (2015).
9. A. Zaviyalov, R. Iliew, O. Egorov, and F. Lederer, "Lumped versus distributed description of mode-locked fiber lasers," J. Opt. Soc. Am. B **27**, 2313–2321 (2010).
10. D. J. Kedziora, A. Ankiewicz, and N. Akhmediev, "Triangular rogue wave cascades," Phys. Rev. E **86**, 056602 (2012).

11. C. Kumar, R. Gupta, A. Goyal, S. Loomba, T. S. Raju, and P. K. Panigrahi, "Controlled giant rogue waves in nonlinear fiber optics," Phys. Rev. A **86**, 025802 (2012).
12. A. Ankiewicz, D. J. Kedziora, and N. Akhmediev, "Rogue wave triplets," Phys. Lett. A **375**, 2782–2785 (2011).
13. S. K. Gupta and A. K. Sarma, "Solitary waves in parity-time (PT)–symmetric Bragg grating structure and the existence of optical rogue waves," Europhys. Lett. **105**, 44001 (2014).
14. W.-P. Zhong, L. Chen, M. Belić, and N. Petrović, "Controllable parabolic-cylinder optical rogue wave," Phys. Rev. E **90**, 043201 (2014).
15. J. M. Dudley, G. Genty, and B. J. Eggleton, "Harnessing and control of optical rogue waves in supercontinuum generation," Opt. Express **16**, 3644–3651 (2008).
16. C.-Q. Dai, G.-Q. Zhou, and J.-F. Zhang, "Controllable optical rogue waves in the femtosecond regime," Phys. Rev. E **85**, 016603 (2012).
17. A. Ankiewicz and N. Akhmediev, "Rogue wave solutions for the infinite integrable nonlinear Schrödinger equation hierarchy," Phys. Rev. E **96**, 012219 (2017).
18. Y. Ohta and J. Yang, "General high-order rogue waves and their dynamics in the nonlinear Schrödinger equation," Proc. R. Soc. A **468**, 1716–1740 (2012).
19. J. He, H. Zhang, L. Wang, K. Porsezian, and A. Fokas, "Generating mechanism for higher-order rogue waves," Phys. Rev. E **87**, 052914 (2013).
20. B. Kibler, J. Fatome, C. Finot, G. Millot, G. Genty, B. Wetzel, N. Akhmediev, F. Dias, and J. M. Dudley, "Observation of Kuznetsov-Ma soliton dynamics in optical fibre," Sci. Rep. **2**, 463 (2012).
21. P. Walczak, S. Randoux, and P. Suret, "Optical rogue waves in integrable turbulence," Phys. Rev. Lett. **114**, 143903 (2015).
22. A. N. Pisarchik, R. Jaimes-Reátegui, R. Sevilla-Escoboza, G. Huerta-Cuellar, and M. Taki, "Rogue waves in a multistable system," Phys. Rev. Lett. **107**, 274101 (2011).
23. C. Bonatto, M. Feyereisen, S. Barland, M. Giudici, C. Masoller, J. R. R. Leite, and J. R. Tredicce, "Deterministic optical rogue waves," Phys. Rev. Lett. **107**, 053901 (2011).
24. S. A. Kolpakov, H. Kbashi, and S. V. Sergeyev, "Dynamics of vector rogue waves in a fiber laser with a ring cavity," Optica **3**, 870–875 (2016).
25. S. V. Sergeyev, H. Kbashi, N. Tarasov, Y. Loiko, and S. A. Kolpakov, "Vector-resonance-multimode instability," Phys. Rev. Lett. **118**, 033904 (2017).
26. A. Zaviyalov, O. Egorov, R. Iliew, and F. Lederer, "Rogue waves in mode-locked fiber lasers," Phys. Rev. A **85**, 013828 (2012).
27. M. Anderson, Y. Wang, F. Leo, S. Coen, M. Erkintalo, and S. Murdoch, "Super cavity solitons and the coexistence of multiple nonlinear states in a tristable passive kerr resonator," arXiv: 1702.00782 (2017).
28. A. I. Korytin, A. Y. Kryachko, and A. M. Sergeev, "Dissipative solitons in the complex ginzburg-landau equation for femtosecond lasers," Radiophys. Quantum Electron. **44**, 428–442 (2001).
29. E. Kelleher and J. Travers, "Chirped pulse formation dynamics in ultra-long mode-locked fiber lasers," Opt. Lett. **39**, 1398–1401 (2014).
30. J. Peng, N. Tarasov, S. Sugavanam, and D. Churkin, "Rogue waves generation via nonlinear soliton collision in multiple-soliton state of a mode-locked fiber laser," Opt. Express **24**, 21256–21263 (2016).
31. J. Soto-Crespo, P. Grelu, and N. Akhmediev, "Dissipative rogue waves: extreme pulses generated by passively mode-locked lasers," Phys. Rev. E **84**, 016604 (2011).
32. C. Lecaplain, P. Grelu, J. Soto-Crespo, and N. Akhmediev, "Dissipative rogue waves generated by chaotic pulse bunching in a mode-locked laser," Phys. Rev. Lett. **108**, 233901 (2012).
33. S. Randoux and P. Suret, "Experimental evidence of extreme value statistics in raman fiber lasers," Opt. Lett. **37**, 500–502 (2012).
34. K. Goda and B. Jalali, "Dispersive fourier transformation for fast continuous single-shot measurements," Nat. Photonics **7**, 102–112 (2013).
35. K. Goda, D. R. Solli, K. K. Tsia, and B. Jalali, "Theory of amplified dispersive fourier transformation," Phys. Rev. A **80**, 043821 (2009).
36. A. Mahjoubfar, D. V. Churkin, S. Barland, N. Broderick, S. K. Turitsyn, and B. Jalali, "Time stretch and its applications," Nat. Photonics **11**, 341–351 (2017).
37. K. K. Tsia, K. Goda, D. Capewell, and B. Jalali, "Simultaneous mechanical-scan-free confocal microscopy and laser microsurgery," Opt. Lett. **34**, 2099–2101 (2009).
38. C. Zhang, Y. Xu, X. Wei, K. K. Tsia, and K. K. Wong, "Time-stretch microscopy based on time-wavelength sequence reconstruction from wideband incoherent source," Appl. Phys. Lett. **105**, 041113 (2014).
39. K. Goda, K. Tsia, and B. Jalali, "Serial time-encoded amplified imaging for real-time observation of fast dynamic phenomena," Nature **458**, 1145–1149 (2009).
40. Y. Xu, X. Wei, Z. Ren, K. K. Wong, and K. K. Tsia, "Ultrafast measurements of optical spectral coherence by single-shot time-stretch interferometry," Sci. Rep. **6**, 27937 (2016).
41. G. Herink, B. Jalali, C. Ropers, and D. Solli, "Resolving the build-up of femtosecond mode-locking with single-shot spectroscopy at 90 MHz frame rate," Nat. Photonics **10**, 321–326 (2016).
42. P. Suret, R. El Koussaifi, A. Tikan, C. Evain, S. Randoux, C. Szwaj, and S. Bielawski, "Single-shot observation of optical rogue waves in integrable turbulence using time microscopy," Nat. Commun. **7**, 13136 (2016).
43. A. Klein, T. Yaron, S. Shahal, G. Masri, H. Duadi, and M. Fridman, "Temporal depth imaging," Optica **4**, 502–506 (2017).
44. A. Klein, S. Shahal, G. Masri, H. Duadi, and M. Fridman, "Four wave mixing-based time lens for orthogonal polarized input signals," IEEE Photon. J. **9**, 7102707 (2017).
45. T. Yaron, A. Klein, H. Duadi, and M. Fridman, "Temporal superresolution based on a localization microscopy algorithm," Appl. Opt. **56**, D24–D28 (2017).
46. M. Fridman, Y. Okawachi, S. Clemmen, M. Ménard, M. Lipson, and A. L. Gaeta, "Waveguide-based single-shot temporal cross-correlator," J. Opt. **17**, 035501 (2015).
47. M. Fridman, A. Farsi, Y. Okawachi, and A. L. Gaeta, "Demonstration of temporal cloaking," Nature **481**, 62–65 (2012).
48. A. Klein, H. Duadi, and M. Fridman, "Full-stokes temporal imaging," Opt. Lett. **43**, 1651–1653 (2018).
49. P. Ryczkowski, M. Närhi, C. Billet, G. Genty, and J. Dudley, "Real-time measurements of dissipative solitons in a mode-locked fiber laser," arXiv: 1706.08571 (2017).
50. M. Närhi, B. Wetzel, C. Billet, S. Toenger, T. Sylvestre, J.-M. Merolla, R. Morandotti, F. Dias, G. Genty, and J. M. Dudley, "Real-time measurements of spontaneous breathers and rogue wave events in optical fibre modulation instability," Nat. Commun. **7**, 13675 (2016).
51. N. K. Fontaine, R. P. Scott, L. Zhou, F. M. Soares, J. Heritage, and S. Yoo, "Real-time full-field arbitrary optical waveform measurement," Nat. Photonics **4**, 248–254 (2010).
52. O. Pottiez, R. Paez-Aguirre, J. Cruz, M. Andrés, and E. Kuzin, "Statistical characterization of the internal structure of noiselike pulses using a nonlinear optical loop mirror," Opt. Commun. **377**, 41–51 (2016).
53. J. M. Dudley, G. Genty, F. Dias, B. Kibler, and N. Akhmediev, "Modulation instability, Akhmediev breathers and continuous wave supercontinuum generation," Opt. Express **17**, 21497–21508 (2009).
54. J. M. Soto-Crespo, N. Devine, and N. Akhmediev, "Dissipative solitons with extreme spikes: bifurcation diagrams in the anomalous dispersion regime," J. Opt. Soc. Am. B **34**, 1542–1549 (2017).
55. N. Broderick, M. Erkintalo, and G. Donovan, "Dynamics and statistics of noise-like pulses and rogue waves," in *Advanced Photonics* (Optical Society of America, 2014), paper NTH1A.6.
56. G. M. Donovan, "Dynamics and statistics of noise-like pulses in mode-locked lasers," Physica D **309**, 1–8 (2015).
57. Z.-R. Cai, M. Liu, S. Hu, J. Yao, A.-P. Luo, Z.-C. Luo, and W.-C. Xu, "Graphene-decorated microfiber photonic device for generation of rogue waves in a fiber laser," IEEE J. Sel. Top. Quantum Electron. **23**, 20–25 (2017).
58. S. Birkholz, C. Brée, A. Demircan, and G. Steinmeyer, "Predictability of rogue events," Phys. Rev. Lett. **114**, 213901 (2015).
59. R. Salem, M. A. Foster, A. C. Turner-Foster, D. F. Geraghty, M. Lipson, and A. L. Gaeta, "High-speed optical sampling using a silicon-chip temporal magnifier," Opt. Express **17**, 4324–4329 (2009).
60. B. C. Lima, P. I. Pincheira, E. P. Raposo, L. D. S. Menezes, C. B. de Araújo, A. S. Gomes, and R. Kashyap, "Extreme-value statistics of intensities in a cw-pumped random fiber laser," Phys. Rev. A **96**, 013834 (2017).
61. A. Martinez and Z. Sun, "Nanotube and graphene saturable absorbers for fibre lasers," Nat. Photonics **7**, 842–845 (2013).
62. F. Bonaccorso, Z. Sun, T. Hasan, and A. Ferrari, "Graphene photonics and optoelectronics," Nat. Photonics **4**, 611–622 (2010).